Thermal, Fluid, and Neutronic Analysis of an LEU Nuclear Thermal Propulsion Core

Mark E. M. Stewart[1]
VPL at NASA Glenn Research Center, Cleveland, OH, 44135, USA

This paper describes the use of detailed multidisciplinary fluid/thermal/ structural/neutronic simulations to predict performance of the nuclear fuel elements of a LEU Nuclear Thermal Propulsion rocket reactor. To achieve maximum performance, a rocket reactor's fuel must operate near thermal hydraulic, structural and neutronic limits where multidisciplinary interactions are important. Yet physical testing is expensive, time-consuming and risky. Lower-fidelity correlations (heat transfer) and simulations have always existed for design, and one role of detailed numerical analysis is to confirm correlation validity and accuracy. For complex and subtle issues, detailed numerical simulations may prove their value. The paper gives examples of both of these roles. Limitations of the methods and potential extensions will be explored.

I. Nomenclature

CFD = computational fluid dynamics
Cp = specific heat, J/kg-K
D = coolant channel diameter, m
E = modulus of elasticity, Pa
f_{turb} = turbulent Fanning friction factor, dimensionless
FE = fuel element
g = acceleration due to gravity, m/s^2
I_{sp} = specific impulse, s
ITT, OTT = inner tie tube, outer tie tube and associated coolant passages of moderator element
k = coefficient of thermal conductivity, W/m-K
LEU = low enriched uranium
MCNP = Monte Carlo n-particle transport, a neutronics simulation code
ME = moderator element or tie tube
MOM = method of mixtures, mixture properties by vol% of component materials
MW = molecular weight, g/mol
NTP = nuclear thermal propulsion
p = fuel element channel pitch to diameter ratio
PPF = power peaking factor, ratio of local power density, *Q*, to fuel element average
Pr = Prandtl number
q = heat flux, W/m^2
Q = volumetric heat deposition rate, equivalently power density, W/m^3
r_0, *r* = borehole radius of fuel, radial distance to coolant channel center, m
Re = Reynolds number based on coolant channel diameter
R_u = universal gas constant, J/mol-K
s = half coolant channel pitch, m
SNRE = small nuclear rocket engine
T = temperature, K
TD = theoretical density
y^+ = non-dimensional normal spacing of the grid at the wall in a boundary layer
z = axial distance from channel inlet, m
α, *CTE* = coefficient of thermal expansion (secant method), m/m-K

[1] Senior Research Scientist, AIAA (Senior) Member

γ = ratio of specific heats
μ = Poisson's ratio
ρ = density, kg/m^3
$\overline{\rho U^2}$ = momentum flux, average over channel cross-section, Pa
τ_w = shear stress at the wall, Pa
Subscripts:
b = bulk fluid, refers to a channel average at an axial station
out = outlet
t = thermal
w = wall, fluid-solid interface

II. Introduction

NASA's Game Changing Development (GCD) program has undertaken a conceptual design study of a Low Enriched Uranium (LEU) Nuclear Thermal Propulsion (NTP) rocket reactor. The reactor design lead is BWXT Technologies. Although NTP engines have been developed and tested in the past, this LEU engine promises a significantly reduced risk of nuclear proliferation, due to the low enrichment of its uranium fuel, namely less than 20% versus greater than 90 atom% U_{235} for its predecessors. With 20% of the fissionable target atoms, an LEU design is challenging. Neutrons must be conserved by excluding neutron absorbing materials, limiting leakage, sizing the reactor, and using relatively large volumes of neutron moderating material. Similarly, the CANDU reactor also trades uranium enrichment (natural uranium fuel) for low neutron absorption materials, reactor size and large moderator volume (heavy water).

Nuclear thermal rockets have the promise of high levels of thrust while efficiently using propellant. Uniquely for a rocket, nuclear heat is deposited in the solid fuel, diffuses to nearby coolant channels containing flowing propellant; fuel is cooled, propellant is heated. In contrast, chemical rocket engines release heat directly into the gas phase; incidentally, walls are carefully cooled. Electric propulsion accelerates ions in an electric field—not thermally, but, their prodigious efficiency, I_{sp}, does not include high thrust.

The propulsion advantage of NTP comes from the molecular weight (*MW*) of the hydrogen propellant; Eq. (1) gives specific impulse, I_{sp}. Hydrogen has *MW* = 2 g/mol, while a chemical rocket's water vapor propellant—from burning hydrogen and oxygen—has *MW* = 18 g/mol. In principle, specific impulse, I_{sp}, is three times higher; practically, fuel melting temperature limits I_{sp} to twice that of the best chemical rockets, 800-900 s.

$$I_{sp} = \frac{1}{g}\sqrt{2\,\frac{\gamma\,R_u}{(1-\gamma)MW}\,T_{out}} \tag{1}$$

Except for the fuel, NTP engine components (turbopumps, nozzles, control drums) have demonstrated operating performance in proven designs. Hence fuel design is important here[2]. Propulsion efficiency for rocket engines increases with higher coolant (propellant) outflow temperature, T_{out}, in Eq. (1). For I_{sp} = 875 s the propellant temperature exceeds 2500 K; while most of the fuel is cooler, the peak fuel temperature will be hotter, and the fuel must be chemically stable while not melting significantly. Nuclear fuel for commercial reactors does not approach this operating temperature, or the power density required for a compact rocket. Consequently, thermal considerations require short distances (~1 mm) between nuclear heat deposition and cooling propellant. Instead of a terrestrial reactor's solid fuel pellets (~1 cm), fuel elements need coolant channels (1 mm scale) to achieve high power density, non-melting fuel, and high rocket I_{sp}. An important part of NTP fuel element design is dealing with the heat physics in the ~350K between the peak propellant and fuel melting temperatures.

Nuclear thermal rockets were first conceived in 1946 [1]. During the Space Race, the Rover and NERVA programs were initiated in 1955 and 1961 to develop NTP technology. In these programs the KIWI, NRX, PHOEBUS, PEWEE, and NF reactors were designed, built, and tested; excellent histories of graphite reactor development are given in References [2] and [3].

In parallel efforts during the 1960's, fast spectrum reactors with cermet fuel elements were developed to lower technical readiness levels (TRL) than graphite fueled reactors. Considerable basic materials research was done at

[2] Also, demonstration is required that cryocoolers can control boil off of stored liquid hydrogen during long duration spaceflight. Also, tank permeability to hydrogen.

NASA and DOE laboratories to characterize cermet fuel behavior [4], particularly at high temperatures. Argonne National Laboratory designed, but did not test, the ANL200 [5] and ANL2000 engines—200 MW_t and 2000 MW_t fast spectrum propulsion reactors.

By the early 1970's, chemical rockets had become operationally successful, and the initial goals of the Space Race had been achieved. With changing priorities, the programs were cancelled in early 1973. Yet, interest in NTP continues since it may be an enabling technology for crewed inter-planetary missions, among others.

III. Fuel and Reactor Models and Simulation Methods

This thermal, hydraulic, neutronic and structural analysis involves a detailed multidisciplinary simulation of the fuel elements and tie tubes within an NTP rocket reactor core. There are three principle simulation components: reactor neutronic analysis, fluid/thermal simulation of adjacent fuel and moderator elements, and their structural analysis. Each model is outlined in the following sections, with explanations of geometry, grid generation, and required material properties. Further, this high fidelity analysis is compared with preliminary design methods.

These multidisciplinary analysis methods have been used to simulate other NTP engines: the graphite composite (U(Zr,C)-graphite) SNRE [6] from the NERVA program, and the cermet (UO_2/tungsten) ANL200 [7] engine.

These multidisciplinary simulations are independent of the engineering analysis within the GCD program—a valuable confirmation of predictions.

A. Nuclear Rocket Reactor and Neutronic Modeling

The simulated reactor is one of the design iterations in the conceptual design of a LEU NTP engine. Figure 1 shows sectional views of the reactor. The neutronic analysis uses the Monte Carlo N-Particle (MCNP) [8] [9] transport code.

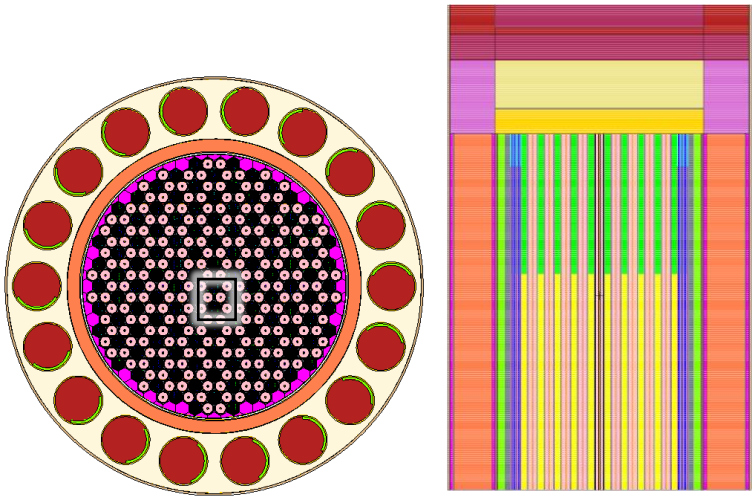

Figure 1: Reactor section views of one Design Analysis Cycle (DAC) of GCD LEU NTP rocket reactor. Radial section (left) and axial-radial section (right). The inset at left corresponds to Figure 2.

The fluid/thermal analysis of the reactor requires, as input, the heat deposition distribution within fuel components. This heat deposition comes from MCNP neutronics simulations. This analysis involves resolving the detailed geometry of the fuel elements and tie tubes within the entire reactor core and modeling the interaction of neutrons with component materials in a Monte Carlo simulation. In particular, the simulation tracks source neutrons, their collisions, fissions, and fission products, using the probability of these events.

Reactor material properties (chemical composition, isotopic fraction, density, theoretical density) are important for these neutronic predictions. They have been carefully developed, and are outlined in Table 1. Further, cross section data for MCNP is needed [10].

In reality, power density varies axially and radially within reactor component; the most important variations, by far, are in the fuel. These include axial variations, local radial variations at an axial station in the fuel element, and variations over all fuel elements in the simulated core. Note carefully that calculated heat deposition, with good statistical validity, is an average—and a high local concentration of power density may be lost to averaging and statistical validity. Note that fuel element edge heating is a variation to include in simulations.

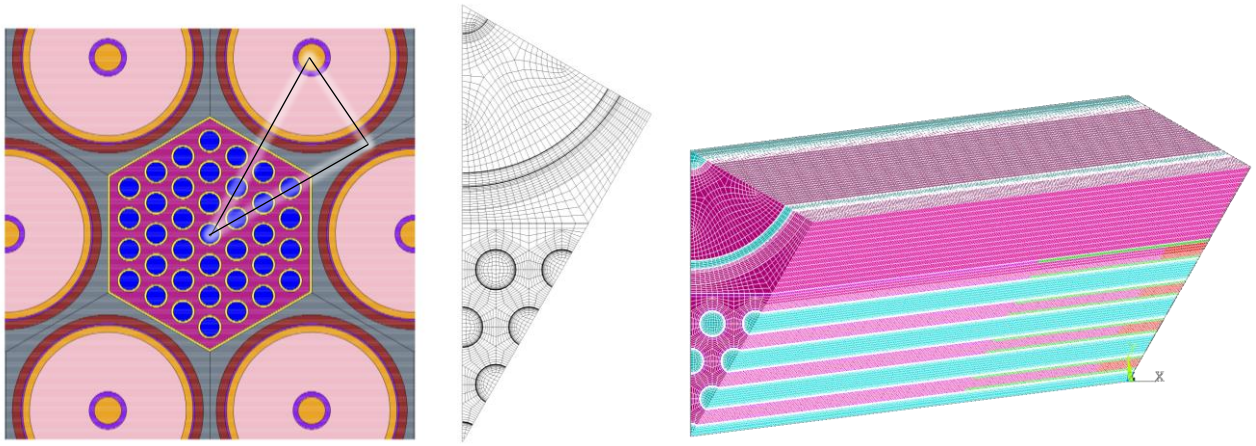

Figure 2: Fuel and moderator element geometry incorporated into a grid. MCNP radial section (left) corresponds to the inset in Figure 1. The inset triangle, at left, is a symmetric sector of the core developed into the grid (center, right) which is full length.

B. Fluid/Thermal Geometry, Grid Generation

Although these simulations are described as a multidisciplinary reactor *core* simulation, the computational cost of the fluid simulation limits this analysis to only part of a fuel element and tie tube. In particular, symmetry is used to reduce the problem to a 30 degree sector fuel element (full-length axial) and a 60 degree sector of an adjacent moderator element (full-length axial), as shown in Figure 2. This symmetry corresponds to a pattern of fuel elements surrounded by moderator elements, Figure 2, which does not exactly match the complex FE/ME placement scheme of some designs.

The grid for a symmetric sector is a composite (non-overlapping) structured grid containing 9.95×10^5 nodes and 1.06×10^6 elements, as shown in Figure 2 center and right. Of these elements, the vast majority are fluid elements. The radial resolution of the solid elements is O(2.5×10^{-4} m). Axially, the grid is full length, and the grid resolution is uniformly 4.52 mm. For ease of grid generation, the complex 2D radial grid (Figure 2, center) is generated with 4 small, simple, 'jigsaw puzzle' grid pieces plus moderator element grids; then this radial grid is axially extruded into a full length grid (Figure 2, right). To reduce numerical error in high gradient regions, the 2D radial grids are designed to keep grid singularities away from the boundary layer, channel coating, and the thermal gradients in the channel walls. The coolant channel coating thickness, the gap spacing, and the high fuel element length-to-width ratio all create high aspect ratio elements.

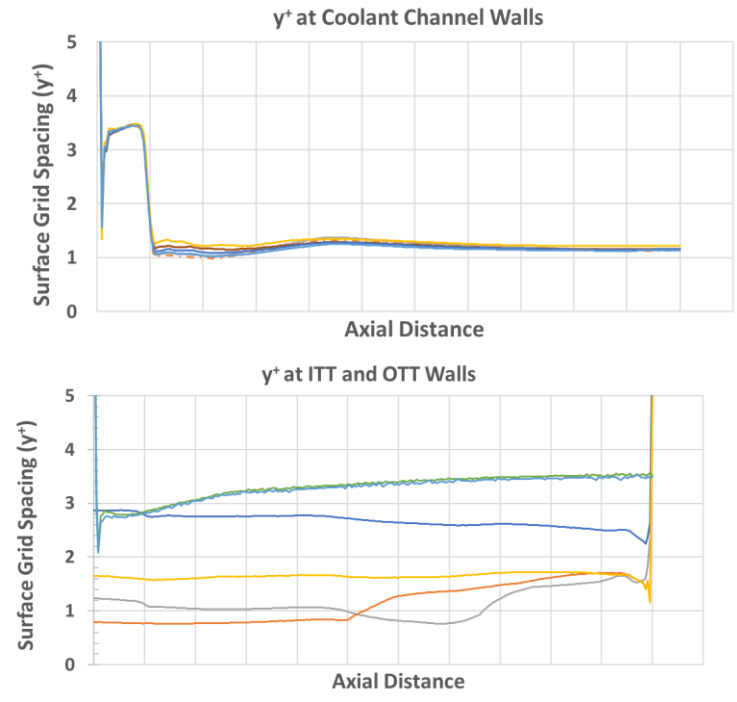

Figure 3: y^+ values measured from the simulation axially along coolant channel walls (above) and along the OTT and ITT walls.

Predicting heat transfer from solid fuel to coolant channel propellant is critical to the design. To capture heat transfer, the fluid simulation solves the thermal and momentum boundary layers, which the grid must resolve. Heat transfer modeling

best practices are surface normal grid spacing at the wall of $y^+ \cong 1$ (physically 1.27 μm), and normal grid spacing increases by a factor of 1.1 away from the wall. As confirmation, Figure 3 shows the measured y^+ values from the simulation. These results were achieved with more than 16 cells across the coolant channel boundary layers, and 38 cells across the OTT passage.

C. Material Properties

Isotropic, temperature dependent material properties are used for each of the FE/ME materials. Figure 4 shows temperature dependent thermal conductivity, *k*, and Figure 5 shows secant coefficient of thermal expansion, α. Table 1 gives the data sources for coefficients of thermal conductivity, *k*, thermal expansion, α, modulus of elasticity, *E*, Poisson's ratio, μ, and specific heat, C_P.

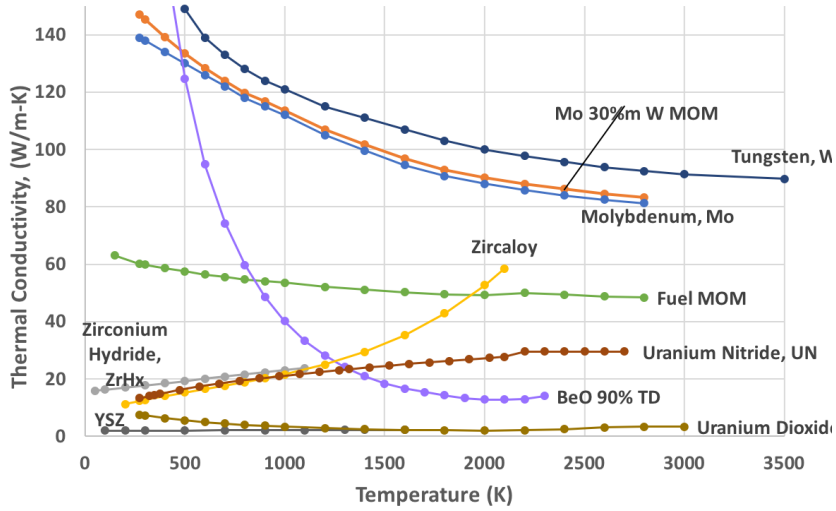

Figure 4: Temperature dependent thermal conductivity functions used in simulations.

Where a stabilizer is used in a material, material properties may revert to the unstabilized material, for example, (CeO_2) 8 mol% ZrO_2 may use the properties of Zirconia, ZrO_2.

1. Sintered, Partially Consolidated, and Particle Materials

Fabrication of fuel elements with fine coolant channels is a challenge, and many approaches have been taken. In the current simulations, materials are assumed to consolidated (not particle), with high theoretical density. The available literature suggests that particle fuel has relatively low thermal conductivity compared with fully consolidated material. 2-10% is supported by the literature [11] [12] [13] [14].

Table 1: Sources for material properties used in simulations. Although there are many sources, these are the best found.

Material	Thermal Conduct, *k*	Thermal Expans, *α*	Elastic Modulus, *E*	Poisson Ratio, *μ*	Specific Heat, C_P	Melting Point (K)	Density, *ρ*
UN	[31] [33]	[32] [33]	[18]	[18]	-	3120	14.3
UO_2	[40] [36]	[40] [36]	[44]	[44]	-	3140	11.0
Mo 30%m W	[33] MOM	[33]	[19]	[19]	-		11.9
W	[33]	[33]	[19]	[19]	-	3695	19.3
Mo	[33]	[33]	[38] [41] [43]	[38] [41]	-	2896	10.2
YSZ	[42]	[42]	[42]	[42]	-	~2970	6.0
Zircaloy-4	[34] [37]	[34] [37]	[37] [41]	[37] [41]	-	2123	6.58
$ZrH_{1.89}$	[33] [35]	[33] [35]	[35]	[35]	-	-	5.62
H_2, Para	[15]	[15]	-	-	[15]	-	[15]
BeO	[39] [33]	[39] [33]	[39]	[39]	-	-	2.86
Reactor / Nuclear Only							
Be						1560	1.85
B_4C							2.52

2. Temperature and Pressure Dependent Hydrogen Properties

The thermodynamic and transport properties of hydrogen are temperature and pressure dependent. Parahydrogen property data are from an NTP program standard [15]. These data are a combination of REFPROP [16] for cryogenic properties, matched to high temperature data. Although ANSYS Multiphysics [17] allows temperature dependent properties, it does not adequately accommodate pressure dependence. Hydrogen properties are specified at a representative pressure.

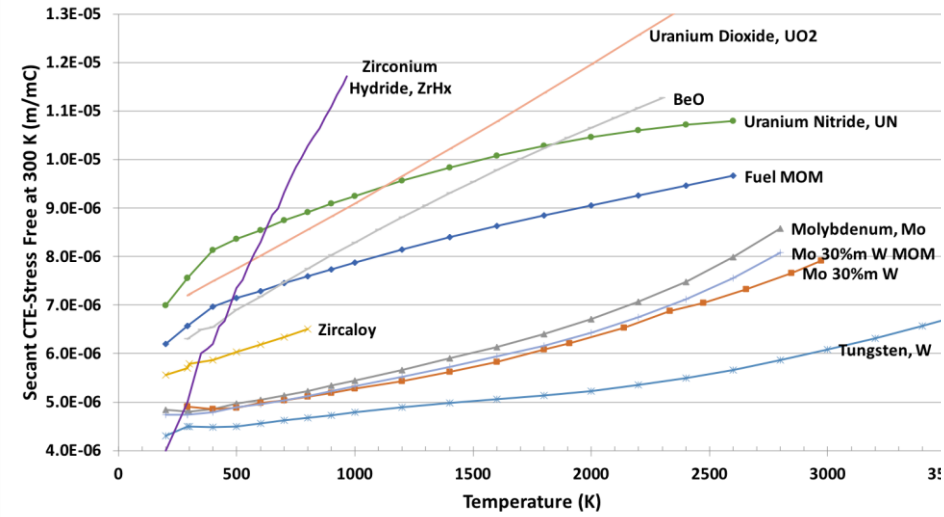

Figure 5: Temperature dependent thermal expansion (secant method) used in simulations. These data are stress free at 300 K; high fabrication temperatures which leave residual stresses during cooling may warrant a different form.

3. Fuel Mechanical Deformation, Plasticity and Creep

Although not part of this work, important references for fuel mechanical deformation, plasticity and creep are: [18] [19] [20] [21]

4. Fuel High Temperature Stability

Although not part of these simulations, important references for high temperature fuel stability are: [22] [23] [24] [25].

D. Fluid and Thermal Models

The steady, incompressible flow through the fuel element coolant tubes and the support element passages is simulated with FLOTRAN which solves the three-dimensional Reynolds Averaged Navier-Stokes (RANS) equations. Turbulence effects are simulated with the κ-ε turbulence closure model.

A common outlet pressure is specified for all coolant channels. The inflow boundary condition for each coolant channel is a constant fluid temperature and axial velocity. The corresponding mass flow is the reactor average mass flow for each channel. All solid walls have a no-slip boundary condition, and the geometrically symmetric boundaries have symmetric fluid boundary conditions. An improvement would be a common pressure drop across all channels. No orificing is included in these simulations, although it was part of the SNRE design [26].

The thermal simulation of the solid material solves the heat equation. Due to symmetry, the external boundaries are treated as adiabatic surfaces.

E. 3D Multidisciplinary Analysis Methodology

The baseline 3D multidisciplinary analysis is ANSYS [17] Multiphysics which combines FLOTRAN for the fluid analysis, ANSYS thermal for the thermal analysis, and ANSYS structural for the stress analysis. First an MCNP analysis provides an axial nuclear heat deposition distribution (volumetric) for each material in the fluid/thermal analysis. Second, the fluid and thermal analyses are performed so that both analyses are consistent—that is, temperatures and heat fluxes match at the fluid-solid interfaces. Third, the structural analysis uses pressures and temperatures from the second analysis to find displacements—and where appropriate, strains and stresses. Currently, feedback—for example, geometry displacements modifying the FE grid—does not occur.

F. Traditional Design Methodology

The contrast between the current 3D multidisciplinary methods and traditional methods is important. Fifty years ago, in the NERVA/Rover program, NTP design analysis techniques focused on correlations, formulae and early particle transport codes. These traditional methods are much faster and simpler; a correlation can be implemented in minutes and checked in hours, but specialized experiments must validate these formulae. In contrast, developing a CFD simulation (generating grids, formulating material properties, checking results) is measured in weeks, if not

months, but these methods are general and can be applied widely across many engineering disciplines. Modern numerical methods solve the fundamental differential equations (Navier-Stokes, heat, stress-strain, Monte Carlo particle transport). In particular, fluid equations and grids resolve the momentum and thermal boundary layers in coolant channels; fuel element edges are resolved to predict temperatures. Consequently, modern numerical methods can detect subtleties in a problem. Since these two approaches are so different, comparing them is an important validation, and this comparison is made in Section IV-C.

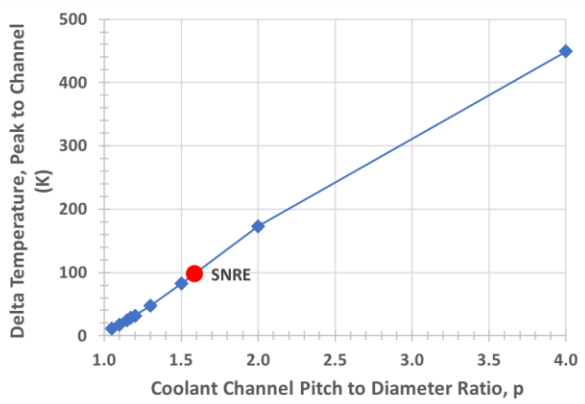

Figure 6: Graph of the Sparrow equation's predictions, Eq. (2), of temperature difference, fuel peak to channel wall temperature. Graph uses conditions, *Q*, *k*, for peak fuel temperature region. The thermal boundary layer has an additional temperature jump.

1. Sparrow Equation for FE Peak Temperature

The Sparrow equation, Eq. (2) [26] is an important, traditional *solution* to the heat equation for predicting fuel temperature. In particular, it quickly reveals the sensitivity of peak fuel temperature to fuel thermal conductivity, *k*, fuel channel pitch, *s*, and heat deposition, *Q*, as shown in Figure 6. It does not include the temperature jump through the thermal boundary layer. For a plausible difference (< 150K) between the peak fuel and wall temperatures, the channel pitch to diameter ratio must be p = 2 or less. However, Eq. (2) works for an infinite array of uniformly spaced coolant channels, and will not predict temperatures—and temperature peaks—at the edges of a fuel element. In Figure 7, it is clear that without the orange virtual channels cooling the fuel, the red channels have more fuel to cool—they are overworked. In the NERVA/Rover program, this deficiency was avoided and FE edge temperatures were predicted by solving the heat equation on 2D sections [27, pp. 155, Vol 2].

$$T - T_{wall} = \frac{Q}{k} s^2 \left[\frac{\sqrt{3}}{\pi} \ln\left(\frac{r}{r_0}\right) - \frac{1}{4}\left[\left(\frac{r}{s}\right)^2 - \left(\frac{r_0}{s}\right)^2 \right] + ftn(r, r_0, s, \theta) \right] \quad (2)$$

In Eq. (2), *ftn()* refers to additional Fourier series terms that match zero heat flux on symmetric surfaces.

2. Coolant Channel Wall Heat Transfer

Another important design prediction is heat transfer at coolant channel walls. Traditional heat transfer correlations remain a fast and effective method of predicting the heat transfer at coolant channel walls. Equation 3 gives the SNRE standard formula [27, pp. 138, Vol 2], and there are a number of similar correlations [28] which all fit experimental data [29] to non-dimensional parameters.

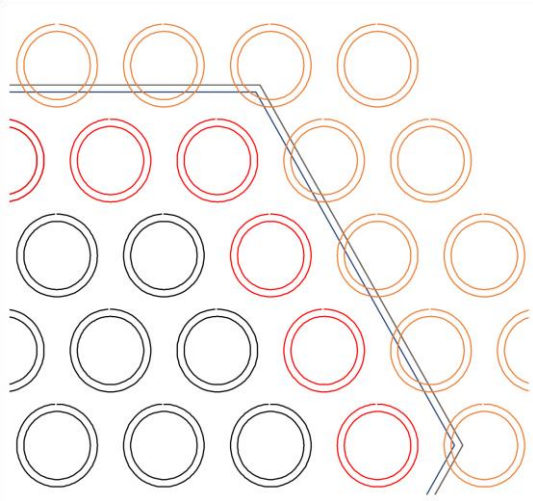

Figure 7: Overworked edge coolant channels, in red. The Sparrow Equation, Eq. (2), assumes an infinite array of coolant channels—not valid at the fuel element edge. Without orange channels, red channels have more fuel to cool.

$$q = 0.023 \frac{k_b}{D_b} {Re_b}^{0.8} {Pr_b}^{0.4} \left(\frac{T_w}{T_b}\right)^{\left[-0.57 - \frac{1.59}{x/D_b}\right]} \quad (3)$$

Coolant channel pressure drop is traditionally predicted with Eq. (4); here the first RHS term, Bernoulli term, is negligible. The Fanning friction factor, f_{turb}, is given by a correlation Eq. (5), and was fitted [30] so that 90% of experimental data fell within ±10%.

$$\Delta p = -\frac{1}{2}\Delta\overline{\rho U^2} - f_{turb}\left(\frac{1}{2}\overline{\rho U^2}\right)\frac{2\,\Delta z}{D_b} \quad (4)$$

$$f_{turb} = \frac{\tau_w}{\frac{1}{2}\overline{\rho U^2}} = \left(0.0014 + \frac{0.125}{Re^{0.32}}\right)\left(\frac{T_b}{T_w}\right)^{1/2} \quad (5)$$

Note that the methods described in this section, F**,** are distinct from the CFD and multidisciplinary methods used in this paper.

IV. Results

The principal results of these fluid / thermal / structural / neutronic simulations are nuclear heat deposition into component materials, coolant exit temperature (and range), maximum fuel temperature and location, temperature distribution through the fuel and moderator, propellant velocity, heat fluxes at coolant tube and moderator passage surfaces (comparison with correlations), FE to ME heat transfer, material thermal expansion and stresses, and the role of fuel thermal conductivity. Figure 8 shows the temperature distribution through the FE and ME.

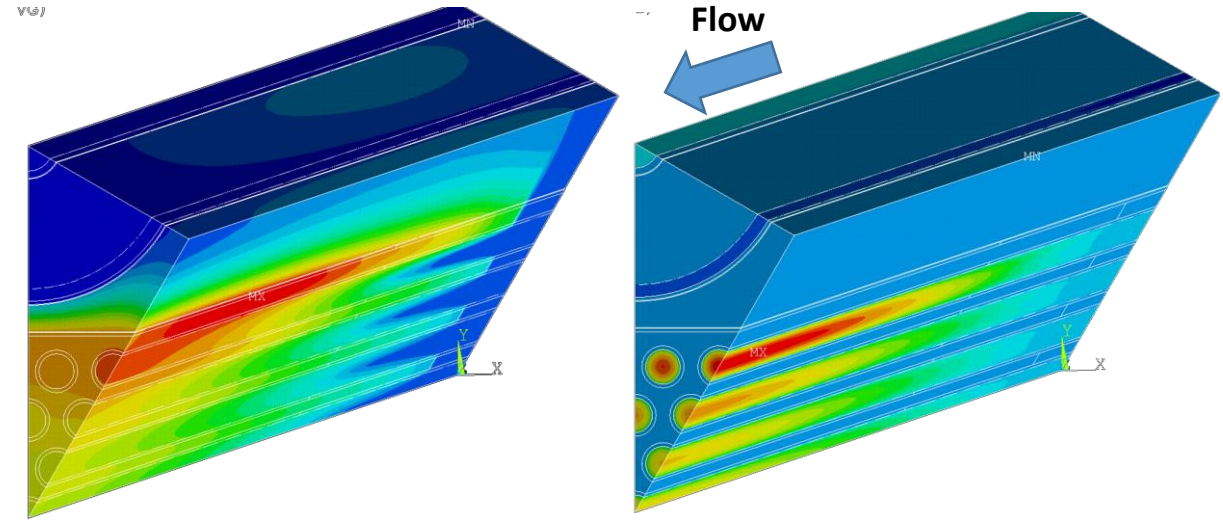

Figure 8: Typical temperature distribution (left) and velocity distribution (right) through fuel and moderator element. Average fuel element with a power peaking factor of *PPF* = 2 on the edge. Thermal and momentum boundary layer development is clear.

A. Neutronic Analysis and Nuclear Heat Deposition

Neutronic analysis using MCNP provides a heat deposition axial profile for each material in the FE/ME model, as shown in Figure 9. The axial distributions come from MCNP tallies for each material (1 cm axial resolution). They are an average over many FEs or MEs, some hotter and some colder than average. No fuel grading is included in these MCNP simulations. The Figure 9 axial profiles are scaled to the reactor power and applied to the thermal/fluid simulations. The fuel heat deposition profile is adjusted upward to include edge heating (Figure 12).

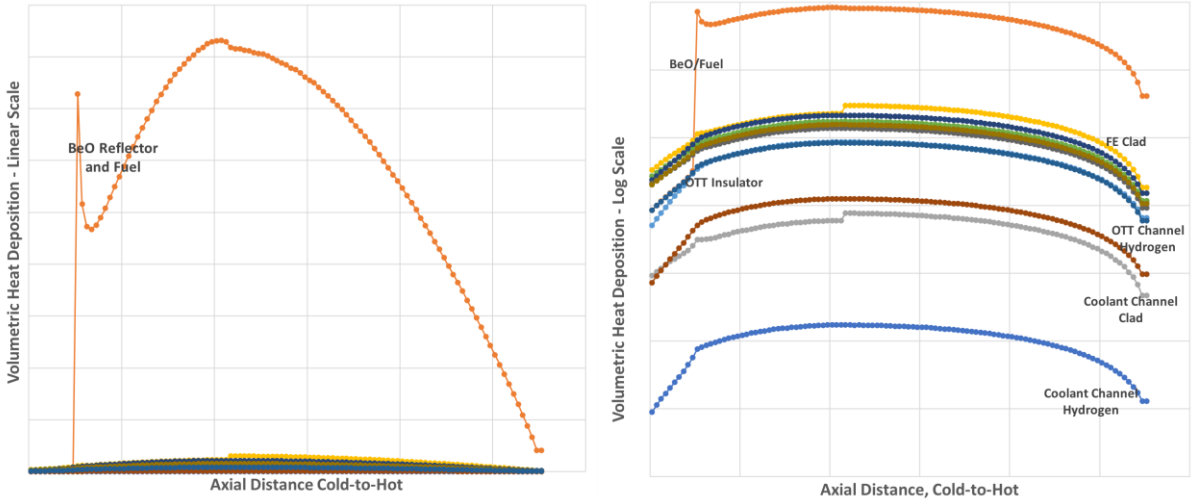

Figure 9: Heat deposition axial profiles from MCNP analysis applied to the fluid/thermal analysis. Linear scale (left) and log scale (right) to show all component materials.

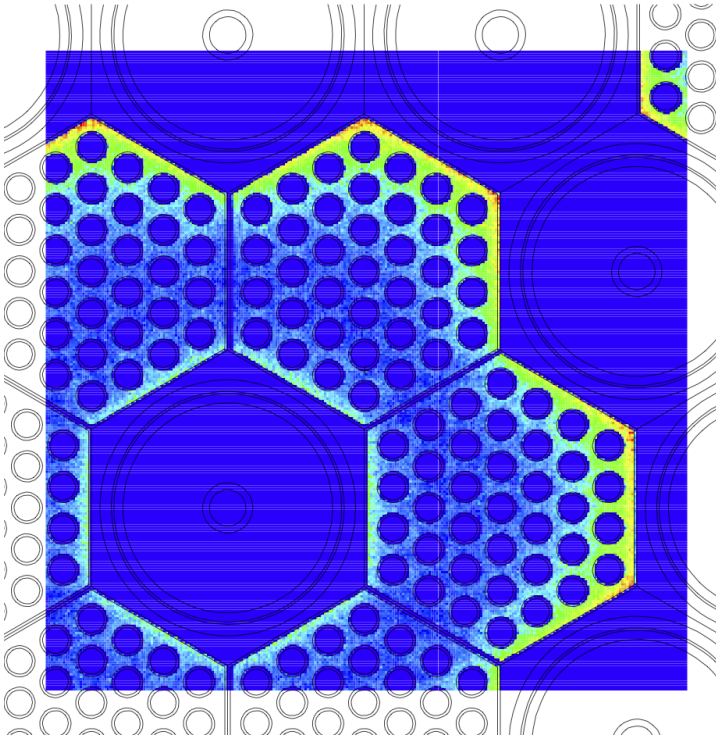

Figure 10: TMESH/MCNP plot of power density in hottest axial 20cm of reactor at the reactor's axial axis. Results are qualitative; linear color scale is a factor of ~3, extreme values are cutoff—to blue.

1. Fuel Element Edge Heating

For a reactor material, particularly fuel, heat deposition varies radially. An important effect occurs when adjacent moderator elements induce a higher thermal neutron flux at the edges of fuel elements. Higher fission and heat deposition rates result near the adjacent fuel element edges. Figure 10 shows these radial heat deposition variations qualitatively. Peak heat deposition appears to occur at FE hexagonal corners. Some FE sides have different heat deposition rates than others. Figure 11 suggests variations across the reactor. No fuel grading was used here, but the SNRE design included radial grading of uranium loading—a factor of three concentration variation [27, p. 96 Vol 2].

Tally averages can be deceptive. With so many averages, how does one find a local peak in nuclear heat deposition? Averages over many FEs or larger volumes improve the statistical validity of Monte Carlo predictions, but do not necessarily quantify local concentrations of nuclear heating. Quantitative predictions are increasingly difficult as tally region volumes decrease and become less statistically valid.

Figure 12 shows the predicted power peaking factor, *PPF*, in nuclear heat deposition rate approaching an average FE element edge. This prediction is statistically valid, and comes from specifying MCNP simulation geometry as a hexagonal prism just inside the hexagonal prism defining the FE fuel (clad is exterior, coolant channels interior). The resulting thin edge hexagonal shell is instrumented with a tally over all fuel elements. By varying the size of the "hex outside a hex" and measuring the heat deposition in this shell, this estimate is made of the average edge heat deposition approaching a FE edge.

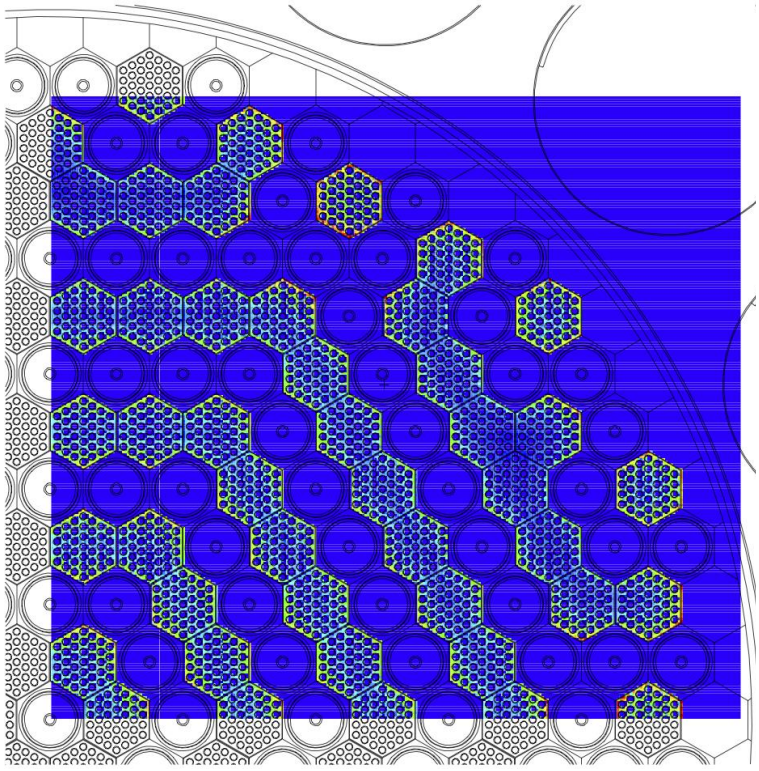

Figure 11: TMESH/MCNP plot of power density in hottest 20cm axial of reactor. Results are qualitative; linear color scale is a factor of ~5, extreme values are cutoff—to blue.

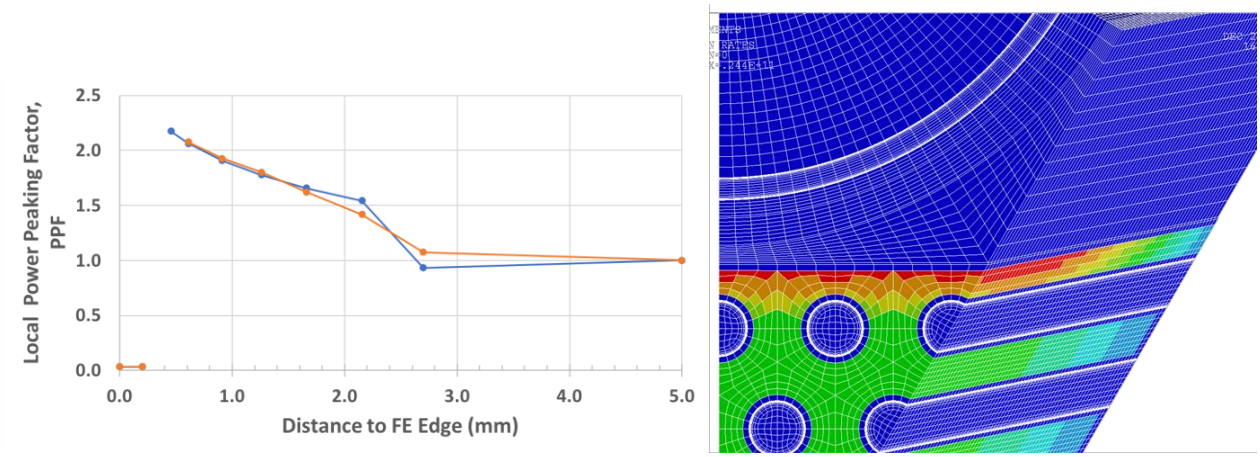

Figure 12: Predicted fuel element power peaking factor, *PPF*, near an average FE edge. Predicted factor (left) and inclusion in the fluid/thermal model as a heat deposition source term (right).

B. Temperature Predictions through Fuel and Moderator Elements

The thermal/fluid simulations predict temperatures throughout the fuel and moderator elements. Figure 13 shows the temperatures along a path through the simulation at six axial stations. The thermal/fluid simulations also give velocity profiles and heat fluxes through fuel and moderator elements. Figure 14 shows velocity profiles, and Figure 15 shows heat flux profiles along coolant channel walls.

The effect of edge heating and edge coolant channels is clear in each of these figures.

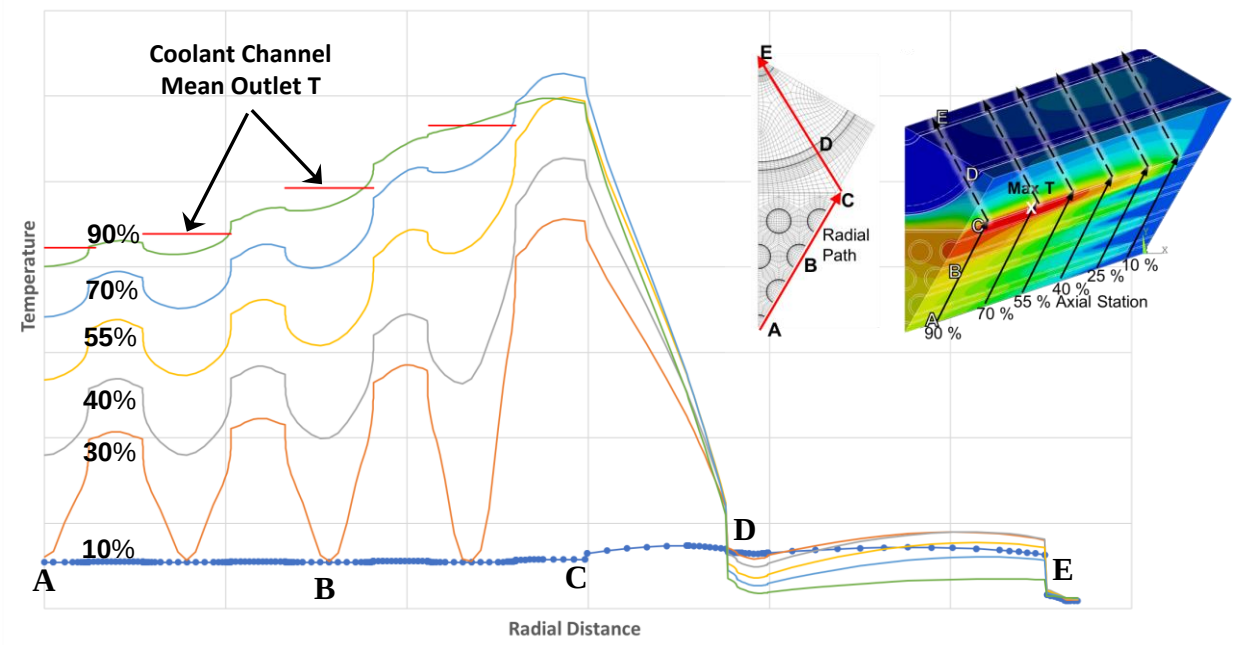

Figure 13: Temperature profiles measured through the fuel element at six axial stations. Specified edge heating is *PPF*=2, as in Figure 12.

C. Heat Transfer Comparison between Correlations and CFD Simulation

Early NTP reactors were designed with heat transfer correlations, Eq. (3) [27, pp. 138, Vol 2], and these correlations remain a fast and effective method of predicting the heat transfer at coolant channel walls, particularly when they have been as carefully developed and validated as they were in the NERVA/Rover program [28] [30].

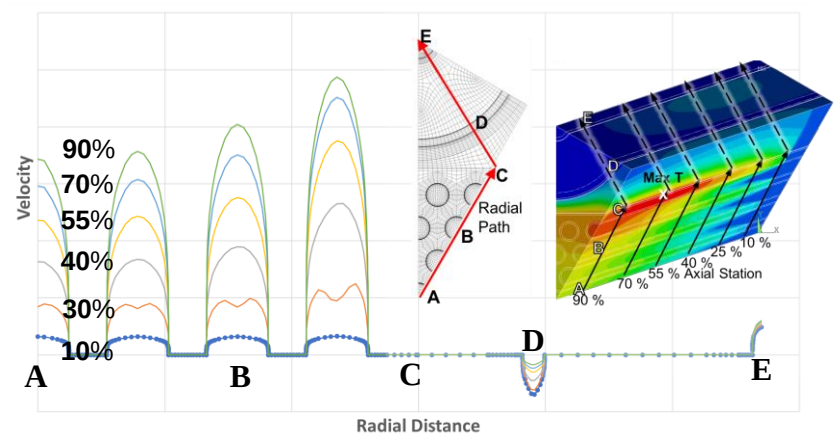

Figure 14: Velocity profiles measured through the fuel element at six axial stations. Profiles are as in Figure 13.

Yet, modern computational methods calculate fluid flow and heat transfer in dramatically different manners—they solve fluid equations in detail through the boundary layer. Hence, CFD provides an additional tool, and a valuable comparison. Figure 16 shows this comparison; in particular, the graph shows the heat flux ratio, namely the ratio of correlation predicted heat flux to this simulation's predicted heat flux. The orange line is a value of 1 which would indicate exact agreement. Values below one, suggest the correlation, Eq. (3), is conservative, that is, correlations under predict the heat transfer, relative to CFD. This margin makes predictions and designs more tolerant of modeling and experimental limitations.

Figure 16 suggests a disagreement of 10% to 30% for the interior coolant channels. Best practice suggests that CFD is doing well to predict heat transfer within 10%.

Figure 16 also indicates that coolant channels near the FE edge are unique. Figure 13 suggests that FE edge effects are having a significant effect. In particular, heat transfer is not symmetrical between the two sides, FE edge and interior

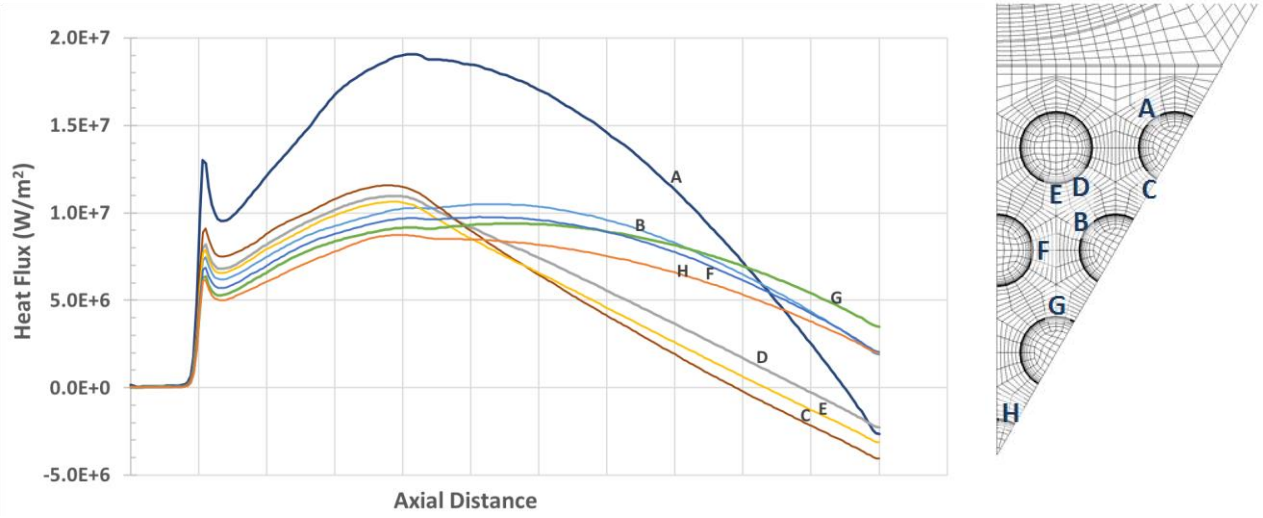

Figure 15: Heat flux measured at eight locations on the fuel element (FE) coolant channel walls. Locations are shown in the map at right. Edge coolant channels deviate from interior channels. Exterior sides at 'A' absorb more heat than interior sides at 'C', 'D' and 'E'.

On the right hand side of Figure 16, several vertical asymptotes occur, and they are not considered significant. Heat transfer is greatly reduced and the two predictions reverse sign at different axial locations leading to vertical asymptotes in the heat flux ratio. Figure 15 shows the reversal of heat flux on the right side in FE edge coolant channels. The clear interpretation is that hot propellant in edge coolant channels at the hot end is heating the fuel.

Note that heat transfer correlations, Eq. (3) and (4), use 'bulk' values—station averages—of fluid temperature, T_b, Reynolds number, Re_b, and Prandtl number, Pr_b, while CFD has detailed profiles across the channel. Further, correlations assume transferred heat is instantly mixed, instead of mixing gradually through the boundary layer and into the bulk.

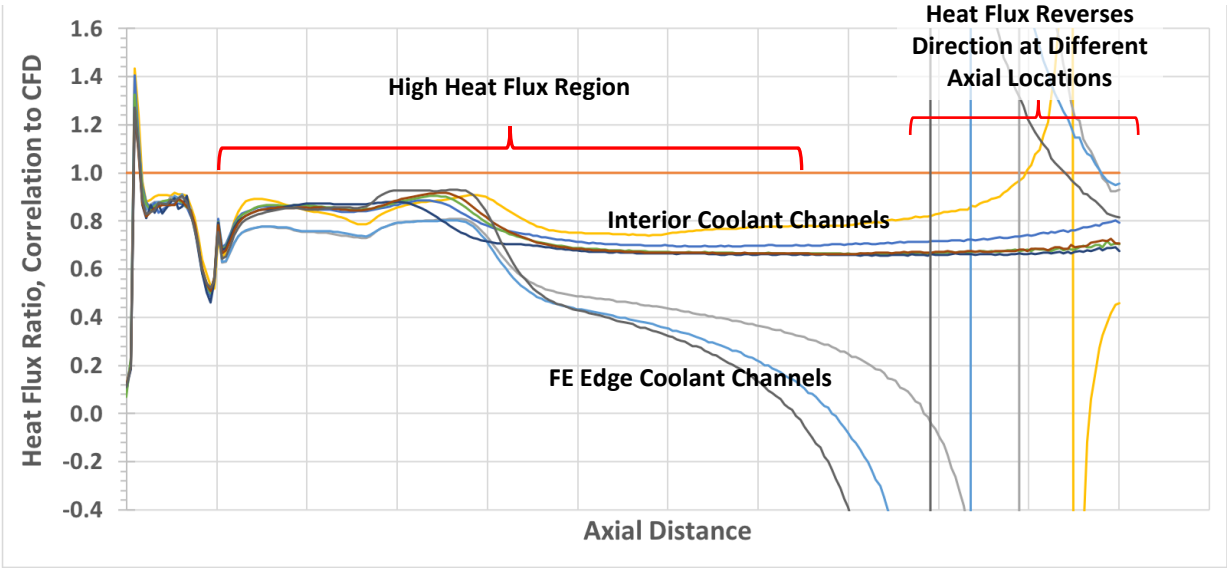

Figure 16: Comparison between heat transfer correlations and CFD by plotting the heat flux ratio. Sample locations are the same as in Figure 15. Edge coolant channels behave differently, as suggested by Figure 13. Vertical asymptotes occur when heat transfer reverses sign at different axial locations, as can be seen in Figure 15.

D. Fuel Element to Moderator Element Heat Transfer

Moderator elements (ME) provide structural support for the reactor core, neutron moderating ZrH_x (x=1.89), plus cooling of this moderator with cryogenic hydrogen flow through axial passages; further this heated hydrogen drives propellant turbopumps. The heat flow into the ME hydrogen is important as it must be properly matched to the turbopumps—in all operational phases—for successful operation of these rocket reactors. Heat conducts (Figure 2, Figure 8, Figure 13) from the FE through multiple materials in the ME, including moderator and high performance insulator layers, annular support tube (tie tube), all with intervening gaps. This model assumes heat conduction

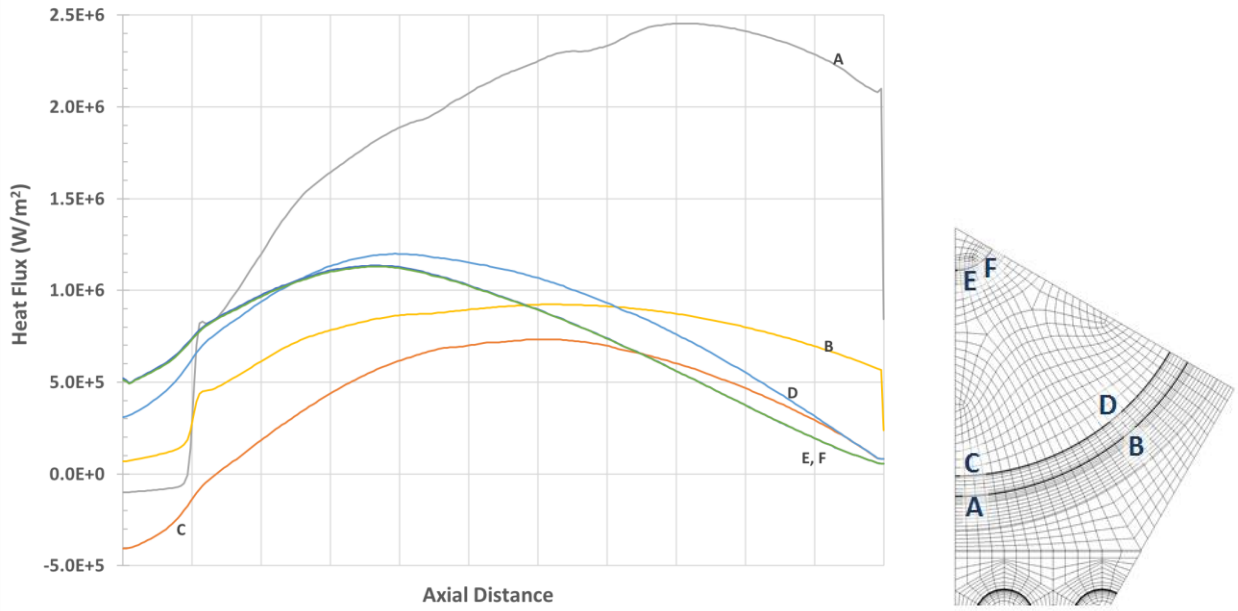

Figure 17: FE to ME heat flux measured at four locations on the moderator element (ME) outer and inner passage walls. The map at right indicates locations.

through uniform thickness gaps (6.35×10^{-5} m) filled with stagnant hydrogen gas—no radiative heat transfer. Figure 17 plots the predicted heat flux at the walls of the annular hydrogen passages in the ME, and Figure 8 and Figure 13 show the temperature distribution in the outer part of the ME.

For this simulation, 5% of the heat deposited into the FE is transferred to the ME. In the SNRE design [27] and simulations [6] the comparable SNRE value was 6%.

Conclusion

"Longest pole in the tent" is a common expression for 'the problem holding everything up' in a development project, while consuming time, money and patience. The hope of this paper—and the entire design team's work—is to simulate a design thoroughly enough, early enough to understand the physics, fabrication, and cost well enough to avoid issues that delay the project during full development.

Acknowledgments

This work was supported by Game Changing Development Project at NASA Headquarters and the Nuclear Thermal Propulsion program at NASA Marshall Space Flight Center. Computing was provided by Advanced Computing Concepts Lab at NASA Glenn Research Center (GRC). Library services at GRC have been invaluable. This work was not done in isolation; the author thanks Stanley Borowski, Jim Fittje, Tom Lavelle, Justin Milner, Paul Giel, Andy Presby, and Dan Falkenbach at NASA Glenn for many valuable discussions. The author also thanks Jonathan Witter, Michael Eades, Vishal Patel and Jeremy Gustafson for valuable discussions.

References

[1] R. W. Bussard, "Nuclear Powered Rockets: A Historical Survey and Literature Summary," LANL Report LA-2036, Los Alamos, 1956.

[2] D. R. Koenig, "Experience Gained from the Space Nuclear Rocket Program (Rover)," LA-10062-H, Los Alamos National Lab., Los Alamos, NM, May 1986.

[3] J. M. Taub, "A Review of Fuel Element Development for Nuclear Rocket Engines," Los Alamos National Lab., LA-5931, Los Alamos, NM, June 1975.

[4] D. R. deHalas, A. F. Lietzke, N. T. Saunders, C. P. Blankenship, R. E. Gluyas and G. K. Watson, "Reactor and Materials Technology Department: Tungsten-Uranium Dioxide Cermet Research and Development Activities," NASA-CR-54409, BNWL-110, 1965.

[5] Argonne National Laboratory, "Nuclear Rocket Program Terminal Report," ANL-7236, Argonne, IL, 1968.

[6] M. E. M. Stewart and B. G. Schnitzler, "Thermal Hydraulics and Structural Analysis of the Small Nuclear Rocket Engine (SNRE) Core," in *43rd Joint Propulsion Conference*, AIAA 2007-5619, Cincinnati, July 2007.

[7] M. E. M. Stewart and B. G. Schnitzler, "Thermal, Fluid, and Structural Analysis of a Cermet Fuel Element," in *48th Joint Propulsion Conference*, AIAA 2012-3959, Atlanta GA, August 2012.

[8] Los Alamos National Laboratory, "A General Monte Carlo N-Particle (MCNP) Transport Code," [Online]. Available: https://mcnp.lanl.gov. [Accessed 2019].

[9] Los Alamos National Laboratory, "MCNP6 User's Manual Version 1.0," LA-CP-13-00634, Los Alamos, 2013.

[10] "Listing of Available ACE Data Tables: Formerly Appendix G of the MCNP Manual," LANL, LA-UR-17-20709, 2017.

[11] M. J. Ades and K. L. Peddicord, "A Model for Effective Thermal Conductivity of Unrestructured Sphere-Pac Fuel," *Nuclear Science and Engineering,* vol. 81, no. 4, pp. 540-555, 1982.

[12] M. J. Ades and K. L. Peddicord, "Effective Thermal Conductivity of Sphere-Pac Fuel During Restructuring," *Nuclear Science and Engineering,* vol. 81, no. 4, pp. 563-569, 1982.

[13] C. Hellwig, F. Ingold, L. A. Nordstrom, K. Bakker, T. Ozawa, M. Nakamura and Y. Kihara, "FUJI--A Comparative Irradiation Test with Pellet, Sphere-Pac and Vipac Fuel," in *Proc. ATALANTE 2004 Conf.*, Nimes, France, 2004.

[14] K. Tanaka, S. Miwa, S.-i. Sekine, H. Yoshimochi, H. Obayashi and S.-i. Koyama, "Restructuring and redistribution of actinides in Am-MOX fuel during the first 24 h of irradiation," *Journal of Nuclear Materials,* vol. 440, pp. 480-488, 2013.

[15] "Private Communication Jonathan McDonald," 2018.

[16] NIST, "Thermophysical Properties of Fluid Systems," National Institute for Standards and Technology, 2011. [Online]. Available: http://webbook.nist.gov/chemistry/fluid. [Accessed January 2015].

[17] ANSYS, "ANSYS Multiphysics Software, Ver. 17.2," ANSYS, Inc., Canonsburg, PA, Aug 2016.

[18] S. L. Hayes, J. K. Thomas and K. L. Peddicord, "Material Property Correlations for Uranium Mononitride II. Mechanical Properties," *Journal of Nuclear Materials,* vol. 171, pp. 271-288, 1990.

[19] V. T. Ababkov and N. N. Morgunova, "Mechanical propertiex of Mo-W alloys," *Metal Science and Heat Treatment,* vol. 15, no. 5, pp. 376-378, May 1973.

[20] General Electric, Nuclear Materials and Propulsion Operation, "710 High-Temperature Gas Reactor Program Summary Report: Volume V-Fuel Element Stress Analysis," GEMP-600, Vol IV, 1968.

[21] J. B. Conway and P. N. Flagella, "Physical and Mechanical Properties of Reactor Materials," General Electric Co., GEMP-1004, Cincinnati, OH, 1969.

[22] J. Bugl and A. A. Bauer, "Phase, Thermodynamic, Oxidation, and Corrosion Studies of the System Uranium-Nitrogen," Battelle Memorial Institute, BMI-1692, Columbus, OH, 1964.

[23] Pratt & Whitney Aircraft, "URANIUM Nitride Fuel Development SNAP-50," AEC Research & Development Report, Middletown CN, 1965.

[24] J. F. Collins and D. L. Newsom, "Evaluations of Uranium Mononitride Cermet Fuel," GEMP-659, 1968.

[25] P. D. Takkunen, "Fabrication of Cermets of Uranium Nitride and Tungsten or Molybdenum from Mixed Powders and from Coated Particles," NASA TN D-5136, Cleveland, 1969.

[26] F. P. Durham, "Nuclear Engine Definition Study Preliminary Report Vol. 1-3," LA-5044-MS, Los Alamos National Lab., Los Alamos, Sept 1972.

[27] E. M. Sparrow, "Temperature Distribution and Heat-Transfer Results for an Internally Cooled, Heat-Generating Solid," *Trans ASME Journal of Heat Transfer,* pp. 389-392, Nov 1960.

[28] G. R. Thomas, "An Interim Study of Single Phase Heat Transfer Correlations Using Hydrogen," Westinghouse Electric Corporation, Astronuclear Lab, WANL-TNR-056, April 1962.

[29] M. F. Taylor, "Experimental Local Heat-Transfer and Average Friction Data for Hydrogen and Helium Flowing in a Tube at Surface Temperatures Up To 5600 R," NASA TN D-2280, Washing, 1964.

[30] M. F. Taylor, "A Method of Correlating Local and Average Friction Coefficients for both Laminar and Turbulent Flow of Gases Through a Smooth Tube with Surface to Bulk Temperature Ratios from 0.35 to 7.35," *Int. J. Heat Mass Transfer,* vol. 10, pp. 1123-1128, 1967.

[31] S. L. Hayes, J. K. Thomas and K. L. Peddicord, "Material Property Correlations for Uranium Mononitride III. Transport Properties," *Journal of Nuclear Materials,* vol. 171, pp. 289-299, 1990.

[32] S. L. Hayes, J. K. Thomas and K. L. Peddicord, "Material Property Correlations for Uranium Mononitride I. Physical Properties," *Journal of Nuclear Materials,* vol. 171, pp. 262-270, 1990.

[33] Y. S. Touloukian, Thermophysical Properties of Matter, vol. 2, New York: IFF/Plenum, 1970.

[34] L. J. Siefken, E. W. Coryell and E. A. Harvego, "MATPRO - A Library of Materials Properties for Light-Water-Reactor Accident Analysis," Idaho National Engineering and Environmental Laboratory, NUREG/CR-6150, Vol. 4, Rev. 2 INEL-96/0422, Idaho Falls, 2001.

[35] M. T. Simnad, "The U-ZrHx Alloy: Its Properties and Use in Triga Fuel," Rept E-117-833, Ga Project No. 4314,, Feb 1980.

[36] International Atomic Energy Agency, "Thermophysical Properties of Materials for Nuclear Engineering: A Tutorial and Collection of Data," IAEA, https://www-pub.iaea.org/MTCD/Publications/PDF/IAEA-THPH_web.pdf , Vienna, 2008.

[37] C. L. Whitmarsh, "Review of Zircaloy-2 and Zircaloy-4 Properties Relevant to N.S. Savannah Reactor Design," ORNL-3281, Oak Ridge TN, 1962.

[38] X. J. Yu and K. S. Kumar, "The tensile response of Mo, Mo-Re and Mo-Si solid solutions," *Int. Journal of Refractory Metals and Hard Materials,* vol. 41, pp. 329-338, 2013.

[39] S. C. Carnigglia and J. E. Hove, "Fabrication and Properties of Dense Beryllium Oxide," *Journal of Nuclear Materials,* vol. 4, no. 2, pp. 165-176, 1961.

[40] J. K. Fink, M. G. Chasanov and L. Leibowitz, “Thermophysical Properties of Uranium Dioxide,” *Journal of Nuclear Materials,* vol. 102, pp. 17-25, 1981.

[41] "MatWeb Material Property Data," MatWeb, LLC, 2011. [Online]. Available: www.matweb.com. [Accessed 2019].

[42] "Private Communication with BWXT," 2019.

[43] Aerojet Nuclear Systems Company, "Naterials Properties Data Book: Volume 1 - Introduction and Light Metals," Report 2275, 1970.

[44] M. Marlowe, "High Temperature Isothermal Elastic Moduli of UO2," *Journal of Nuclear Materials,* vol. 33, no. 2, pp. 242-244, 1969.